OPTICS

Three-level spaser for next-generation luminescent nanoprobe

Pei Song*, Jian-Hua Wang*, Miao Zhang, Fan Yang, Hai-Jie Lu, Bin Kang†, Jing-Juan Xu†, Hong-Yuan Chen†

The development of modern biological and medical science highly depends on advanced luminescent probes. Current probes typically have wide emission spectra of 30 to 100 nm, which limits the number of resolvable colors that are simultaneously labeled on samples. Spasers, the abbreviation for surface plasmon lasers, have ultranarrow lasing spectra by stimulated light amplification in the plasmon nanocavity. However, high threshold (>10^2 mJ cm^{-2}) and short lasing lifetime (approximately picoseconds to nanoseconds) still remain obstacles for current two-level spaser systems. We demonstrated a new type of a three-level spaser using triplet-state electrons. By prolonging the upper state lifetime and controlling the energy transfer, high gain compensation was generated. This probe, named delayed spasing dots (dsDs), about 50 to 60 nm in size, exhibited a spectral linewidth of ~3 nm, an ultralow threshold of ~1 mJ cm^{-2}, and a delayed lasing lifetime of ~10^2 μs. As the first experimental realization of the three-level spaser system, our results suggested a general strategy to tune the spasing threshold and dynamics by engineering the energy level of the gain medium and the energy transfer process. These dsDs have the potential to become new-generation luminescent probes for super-multiplex biological analysis without disturbance from short lifetime background emission.

INTRODUCTION

Application of luminescent probes, including fluorescent dyes and proteins (*1*, *2*), semiconductor nanocrystals (that is, quantum dots) (*2*, *3*), upconversion nanoparticles (*4*, *5*), and bioluminescent molecules (*6*), has created incalculable value in the fields of biological science, medical science, and chemical industry (*7*). In past decades, scientists have never stopped seeking new probes with novel luminescent properties. One goal is to narrow down the emission spectra. Typically, fluorescent dyes and proteins exhibit broad emission spectra of about 50 to 100 nm (*1*, *2*), and semiconductor and upconversion nanoparticles have narrower spectra, but still in the range of 30 to 50 nm (*3*–*5*). The broad spectra largely limit the number of resolvable colors, typically four to five at most, that are simultaneously labeled on the sample. Another goal is to engineer the emission lifetime (*8*, *9*). Probes with relative long lifetimes could remarkably avoid the background, because most background emission from endogenous molecules in the cell or tissue decays in nanoseconds (*10*).

The first goal naturally brings to mind a special emission with ultranarrow spectra in the range of ~1 to 2 nm, that is, the stimulated emission in a laser (*11*). If the laser size could scale down to nanosize, then the above problem might be solved and many promising applications that are seemingly impossible today could be rebooted. Unfortunately, the physical size of the photonic cavity cannot be smaller than a half-wavelength in theory (*11*), and it usually requires several to tens of micrometers in practice to compensate for the loss of light (*12*–*14*), which is obviously too large for biological probes. It is also possible to amplify light through random light scattering in the gain medium, termed random lasing (*15*–*17*). Intracellular random microlasing was realized by injecting special gain materials into cells to form a microresonator (*18*). However, these microresonators were still too large (≥4 to 10 μm) for biological labeling.

A promising way to further shrink the laser size is to replace the light wave in the cavity with the charge density wave, termed surface plasmon laser or spaser (*19*, *20*). The physical size of a spaser can be down to a few nanometers, in principle, and the lasing action could be supported by either propagating or localized surface plasmon (*21*). Propagating plasmon spasers have been achieved in semiconductors placed on a plasmon substrate (*21*–*25*), which were more like devices, not probes. Spasers based on localized surface plasmon offer instinctive feedback and make it possible to build up a stand-alone lasing emitter on single nanoparticles (*26*, *27*). Although the potential of a single-particle spaser was highly expected in biological applications (*28*, *29*), until now only a couple of works occurred since the first demonstration in 2009 (*28*, *30*). The main obstacles are the low *Q* factor (~15) of the single-particle cavity (*26*), high ohmic loss, and short plasmon retention lifetime (femtoseconds to picoseconds) (*21*). To achieve population inversion and compensate for the loss, very high pump energy (>10^2 mJ cm^{-2}) was typically required (*21*, *28*, *30*). This high threshold largely weakens the potentials of its application as biological probes, especially for living cells. In addition, because of the short energy retention time in the cavity, this type of spaser was predicted to emit a short pulse (approximately picoseconds to nanoseconds) (*21*, *26*, *30*). This short lifetime might be great for ultrafast optics, but it is terrible for biological probes because the signals would be mostly masked under the background emission with a similar lifetime.

Here, inspired by classical laser theory, we demonstrated a new type of spaser based on a three-level gain system with triplet-state electron transition, named delayed spasing dots (dsDs). The long lifetime of the triplet state (~10^1 to 10^2 μs) provides an orders of magnitude increase on population inversion probability. In addition, because of the spin forbidden transition from the singlet state to the triplet state, loss caused by the stimulated absorption in the gain medium was almost eliminated. These two aspects remarkably reduced the pump threshold (~1 mJ cm^{-2}) compared to previous two-level spaser systems (>10^2 mJ cm^{-2}). Finally, the lasing action was realized with an ultranarrow emission spectrum

State Key Laboratory of Analytical Chemistry for Life Science and Collaborative Innovation Center of Chemistry for Life Sciences, School of Chemistry and Chemical Engineering, Nanjing University, 163 Xianlin Road, Nanjing 210023, P. R. China.
*These authors contributed equally to this work.
†Corresponding author. Email: binkang@nju.edu.cn (B.K.); xujj@nju.edu.cn (J.-J.X.); hychen@nju.edu.cn (H.-Y.C.)

(~3 nm), alone with a delayed emission dynamics in ~10^2 μs, which is orders of magnitude longer than previous two-level spasers (approximately picoseconds to nanoseconds). Moreover, the process of energy transfer and the following lasing action was studied by using broadband time-resolved emission spectroscopy (fig. S1) and transient absorption spectroscopy.

RESULTS AND DISCUSSION

Scheme 1 shows a three-level spaser, which is composed of a three-level gain medium and a plasmon cavity. The threshold of a spaser system has been suggested as (*20*, *31*, *32*):

$$\frac{4\pi\mu^2\tau_1}{3h}\cdot\frac{N_1-N_0}{V_{\mathrm{mode}}}\cdot Q\geq 1 \qquad (1)$$

where μ and τ_1 are the excited dipole matrix element and relaxation time, respectively; N_1 and N_0 are the number of quantum emitters on the upper and lower lasing states, respectively; Q is the mode quality factor; and V_{mode} is the mode volume. From the above equation, it is possible to achieve threshold by prolonging the upper state lifetime, increasing population inversion, shrinking mode volume, and using a high Q cavity. Many previous works have developed a high Q cavity (*33*, *34*), yet little attention was focused on the gain medium. For the single-particle cavity, it did not have much room to improve Q due to the highly confined plasmon mode (*20*, *21*, *27*). However, there are still many possibilities of engineering the gain system and the energy transfer. It has been theoretically proposed that a three-level gain medium could remarkably reduce the threshold of the spaser (*35*); however, a three-level spaser has not been experimentally realized yet. Here, we used the triplet excited state to construct a three-level spaser system (figs. S2 and S3), analogous to the classic three-level laser (*11*). On the basis of the calculation results and spectral data, we considered that the triplet-state T_2 was used as an upper energy level in our spaser system. The small energy gap between T_2 and the singlet-state S_1 would be beneficial for fast intersystem crossing (approximately picoseconds to nanoseconds) (*36*). In addition, because the lifetime of the T_2 state (~10^1 to 10^2 μs) is much longer than that of the S_1 state (about nanoseconds) (*36*), the T_2 state could store large population of electrons. The optical amplification depends on the energy transfer between the excited dipole in the gain medium and the plasmon polariton in the cavity (*31*, *37*). In the two-level spaser, the energy transfer is bidirectional, the energy transfer from the gain medium to the cavity generated gain, and the reverse caused loss. Although previous works have proposed that plasmon decay in metal dominated the loss (*21*, *26*), some other works suggested that the dipole-dipole coupled energy transfer from the plasmon to the surrounding molecules was nonignorable; as in some case, this energy transfer might fully quench the plasmon polaritons (*38*, *39*). Here, we used the spin forbidden transition from the S_0 state to the T_2 state to block the energy transfer from the plasmon cavity to the gain medium (*36*). This combination of long excited state lifetime and quasi-unidirectional energy transfer finally resulted in a high-efficiency lasing action.

The schematic structure of the as-prepared dsDs is shown in Fig. 1A. The dsDs mainly consist of two portions, the inner gold (Au) nanoparticle (yellow core) and the outer dye-doped SiO_2 shell (green shell), which act as the plasmon cavity and the gain medium, respectively. The nanocavity is ~20 nm in diameter, and the average thickness of the gain layer is ~24 nm [transmission electron microscopy (TEM); Fig. 1B]. The local light density of the state around the nanocavity was simulated by finite-difference time-domain (FDTD) solution (Fig. 1C), which visually shows the plasmon resonance mode at 545 nm. The Au nanoparticles exhibited a relative broad plasmon resonance band from 470 to 560 nm (Fig. 1D, line 1), with a central wavelength of ~524 nm. The maximum absorption of the gain medium (Fig. 1D, line 2) is at ~490 nm, and then a λ = 488-nm pulse laser was selected as the pump source. The emission spectrum of the gain medium (Fig. 1D, line 3) could be reasonably split into two Gaussian peaks, which were assigned to the $S_1 \rightarrow S_0$ emission at ~520 nm (Fig. 1D, dot line 4) with a lifetime of 3.34 ns (Fig. 1E) and to the $T_2 \rightarrow S_0$ emission at ~540 nm (Fig. 1D, dot line 5) with a lifetime of 11.47 μs (Fig. 1F). Under pumping conditions (λ = 488 nm, 5- to 7-ns pulse), a lasing peak with a linewidth of ~3 nm appeared at 545 nm (Fig. 1D, line 6 and inset).

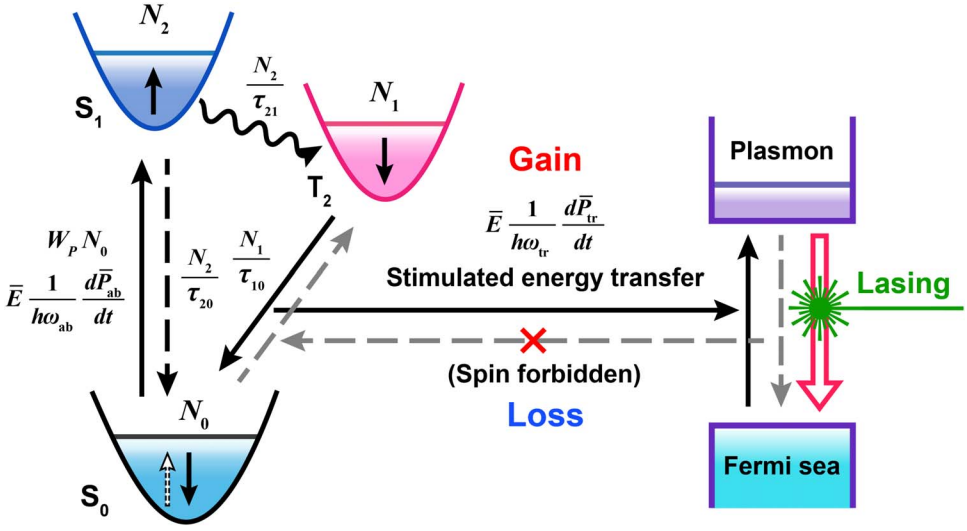

Scheme 1. Conceptual diagram of the three-level spaser.

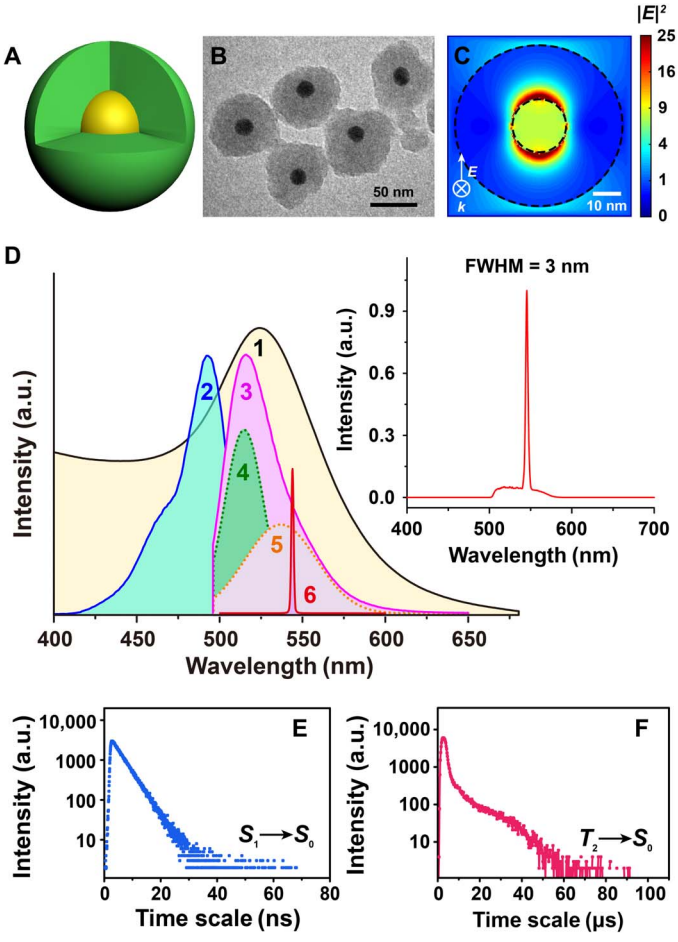

Fig. 1. Demonstration of a three-level spaser. Schematic structure (**A**), TEM (**B**), and FDTD-simulated electric field distribution (**C**) images of the Au@dye/SiO_2 nanoprobe [yellow core and green layer in (A) denote the Au core and the outer dye-doped SiO_2 layer, respectively]. (**D**) Plasmon resonance absorption (1), excitation (2), spontaneous emission (3), split spontaneous emission $S_1 \rightarrow S_0$ (4) and $T_2 \rightarrow S_0$ (5), and stimulated emission (6) curves of the nanoprobe. Inset in (D) is the observed stimulated emission spectrum of the nanoprobe. Emission lifetime of $S_1 \rightarrow S_0$ (**E**) and $T_2 \rightarrow S_0$ (**F**) by using the dye. a.u., arbitrary units; FWHM, full width at half maximum.

We then studied the lasing action under different pump energies (Fig. 2A) using a Nd:YAG laser with λ = 488 nm and 5- to 7-ns pulse width. A laser beam was delivered through a beam expander and roughly covered a 1-cm^2 spot area on a 1-cm cuvette. When the pump energy is below 1 mJ cm^{-2}, a wide band of spontaneous emission was observed. Once the pump energy exceeded a threshold of about 1 mJ cm^{-2}, a narrow lasing peak at 545 nm appeared and quickly dominated over the spontaneous emission (Fig. 2B). Once the lasing action occurred, the linewidth of the emission spectra immediately shrank from 20 to 40 nm to ~3 nm. Here, the threshold of ~1 mJ cm^{-2} is about two orders of magnitude lower than the threshold (>10^2 mJ cm^{-2}) of previous two-level systems (*28*, *30*). As mentioned before, this low threshold could be attributed to the long lifetime of the triplet state and the quasi-unidirectional energy transfer from the gain medium to the cavity. The power intensity under the above threshold is about 10^8 W cm^{-2}, corresponding to a situation of a 1-mW continuous-wave (CW) laser beam tightly focused on a 1-μm spot. This condition could be easily achieved under most confocal microscopes and flow cytometers, which makes it possible to use our dsDs as biological probes compatible with regular instrumentation. To demonstrate that this narrow emission line originated from the spasing action that is amplified by the plasmon cavity, we performed control experiments at the experimental condition similar to that of pumping the spasers by using the gain medium (dye-doped SiO_2) without the plasmon cavity and dye in solution (Figs. 2 and 3 and figs. S4 and S5). As expected, no spasing peak was observed in both of the above samples (Fig. 2C and fig. S5A), which indicated the importance of the plasmon cavity in spasing action. Doping the dyes in SiO_2 nanoparticles modified their spectral features. In dye-doped SiO_2, spectral broadening from a single band of about 520 nm to another band of about 540 nm was observed when pump energy increased from 0.4 to 1.5 mJ cm^{-2} (Fig. 2C). Emission intensity at both 540 and 520 nm, and their intensity ratio ($I_{540\ nm}/I_{520\ nm}$), reached the maximum at a pump energy of about 1 mJ cm^{-2}, which is close to the pumping threshold of the dsDs spaser (Fig. 2D). The spectral evolution suggested an accumulation of excited electrons at the triplet state and a promoted triplet-state emission at high pump energy. These effects were not seen in pump-dependent spectra of dye in solution (fig. S5). The reason might be that, in solution, dye molecules were free of motion and the interaction between molecules was relatively weak, even when the concentration was high. However, when doping dye molecules into SiO_2, the molecular motion was confined and the interaction between molecules could be strong at high dope concentration. In the current spaser system, the accumulation of excited electrons at the triplet state in the gain medium would largely contribute to the population inversion and the final spasing action.

The spasing mechanism in the spaser was proposed as the energy transfer from the gain medium to the plasmon cavity and following optical amplification through coherent plasmon oscillation and feedback (*21*, *31*). Although the spaser theory has been developed for more than 10 years (*19*, *20*), and several spaser systems have been realized (*13*, *23*, *28*), the dynamic process of spasing has not been observed yet. In the current work, we unfolded this process by using a custom-made broadband time-resolved emission spectroscopy system (Fig. 3 and fig. S1). At the initial state of pump (pump energy is 1.5 mJ cm^{-2}), a quench dip of about 545 nm appeared on the emission spectra, which is caused by the energy transfer from electrons at the triplet state to plasmon polaritons. The transfer efficiency is ~90% at 545 nm, and the linewidth of the quench dip is ~10 nm (Fig. 3A). This indicated a stimulated energy transfer driven by a large local density of optical state (LDOS) around nanoparticles (*40*). The quench dip lasted for about 10 μs and began to emit a narrow lasing peak at 545 nm; the lasing peak reached the maximum at 50 to 60 μs and then decayed at ~100 to 150 μs (Fig. 3B). The whole duration of the lasing pulse is ~100 μs with a delay time of ~10 μs. The long lasing retention time suggested a high gain and a low loss, as expected in our design. These unique lasing dynamics offer vital advantages in biological analysis, that is, the background emission from cells or tissues could be largely avoided if a time gate was applied on detection. Time-resolved emission spectral measurement of the gain medium without the (dye-doped SiO_2) plasmon cavity was also performed under the identical experimental conditions (Fig. 3C). No quench dip or spasing peak was observed, except for a delayed fluorescence (τ = 6.6 μs) at 520 nm and phosphorescence at 540 nm (τ = 14.6 μs) (Fig. 3D). Note that fluorescence emission was not detected here because the temporal gate (1 μs) used is not fast enough to capture emission with lifetime of nanoseconds.

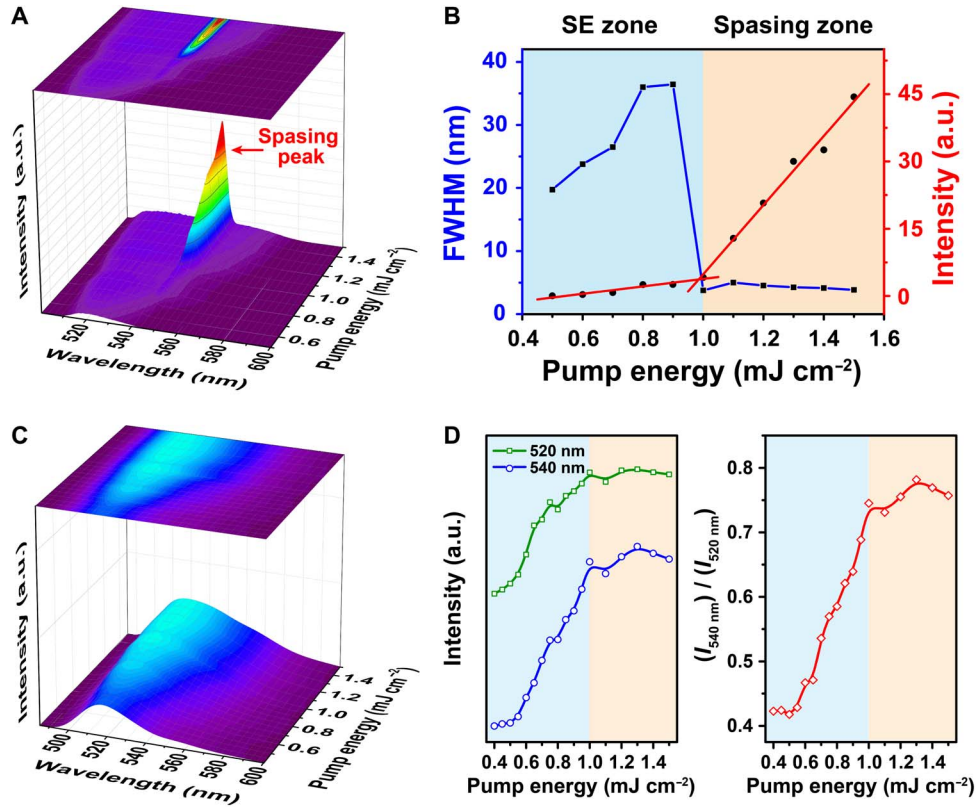

Fig. 2. Ultralow pump threshold of a three-level spaser. (**A**) Emission spectra of the as-prepared dsDs with the pump energy changing from 0.5 to 1.5 mJ cm^{-2}. (**B**) The corresponding FWHM (blue line) and emission intensity (red line) vary with the pump energy. SE, spontaneous emission. (**C**) Emission spectra of the gain material without plasmon cavity under pump energy of 0.4 to 1.5 mJ cm^{-2}. (**D**) Curves of emission intensity at 520 and 540 nm (left) and their ratio (right) with the changing of pump energy.

Our current three-level spaser exhibited two unusual features: ultralow pump threshold (~1 mJ cm^{-2}) and ultralong lasing retention time (~10^2 μs). To better understand the mechanism, we performed a theoretical analysis. According to the Fermi's golden rule, the spontaneous emission could be enhanced by LDOS by the Purcell factor (*41*, *42*).

$$F = \frac{3}{4\pi^2}\left(\frac{Q}{V_{\text{mode}}}\right)\left(\frac{\lambda}{2n}\right)^3 \quad (2)$$

where Q is the cavity quality factor, V_{mode} is the mode volume, λ is the resonance wavelength, and n is the refractive index of the medium. The Purcell effect can increase not only spontaneous emission but also stimulated emission. For the spaser based on a single nanoparticle cavity, the local field density could be increased up to 10^2 to 10^3 times due to the ultrasmall V_{mode}, and F could easily achieve >10^2 (*31*). However, the Q factor for this kind of cavity is low (~15) due to the three-dimensional plasmon confinement (*26*). In addition, because of the fast plasmon decay (approximately picoseconds) in the cavity and the reversible energy transfer between the gain medium and the cavity, high pump threshold (>10^2 mJ cm^{-2}) and short lasing pulse (approximately picoseconds to nanoseconds) were theoretically predicted and experimentally proved (*22*, *26*). Here, we used a three-level gain and controlled the energy transfer, but the whole process should be reevaluated. We considered a three-level gain system with levels <S_0, N_0>, <T_2, N_1>, and <S_1, N_2>, where N_i represents the electron number at each level. Under optical pumping conditions, the occupation numbers of electrons at each energy level vary according to the rate equations (*43*–*45*)

$$\frac{dN_2}{dt} = W_P N_0 + \overline{E}\frac{1}{h\omega_{ab}}\frac{\partial P_{ab}}{\partial t} - \frac{N_2}{\tau_{21}} - \frac{N_2}{\tau_{20}} \quad (3)$$

$$\frac{dN_1}{dt} = \frac{N_2}{\tau_{21}} - \frac{N_1}{\tau_{10}} - \overline{E}\frac{1}{h\omega_{tr}}\frac{\partial P_{tr}}{\partial t} \quad (4)$$

$$\frac{dN_0}{dt} = \frac{N_1}{\tau_{10}} + \frac{N_2}{\tau_{20}} + \overline{E}\frac{1}{h\omega_{tr}}\frac{\partial P_{tr}}{\partial t} - W_P N_0 - \overline{E}\frac{1}{h\omega_{ab}}\frac{\partial P_{ab}}{\partial t} \quad (5)$$

Considering that the system reaches a balance, which is described by $dN_i/dt = 0$. The population can be solved and written as

$$N_2 = \frac{\tau_{21}\tau_{20}}{\tau_{21}+\tau_{20}}\left(W_P N_0 + \overline{E}\frac{1}{h\omega_{ab}}\frac{\partial P_{ab}}{\partial t}\right) \quad (6)$$

$$N_1 = \frac{\tau_{10}\tau_{20}}{\tau_{21}+\tau_{20}}\left(W_P N_0 + \overline{E}\frac{1}{h\omega_{ab}}\frac{\partial P_{ab}}{\partial t}\right) - \overline{E}\frac{\tau_{10}}{h\omega_{tr}}\frac{\partial P_{tr}}{\partial t} \quad (7)$$

$$N_0 = \frac{1}{W_P}\left(\frac{N_2}{\tau_{20}} + \frac{N_1}{\tau_{10}} - \overline{E}\frac{1}{h\omega_{ab}}\frac{\partial P_{ab}}{\partial t} + \overline{E}\frac{1}{h\omega_{tr}}\frac{\partial P_{tr}}{\partial t}\right) \quad (8)$$

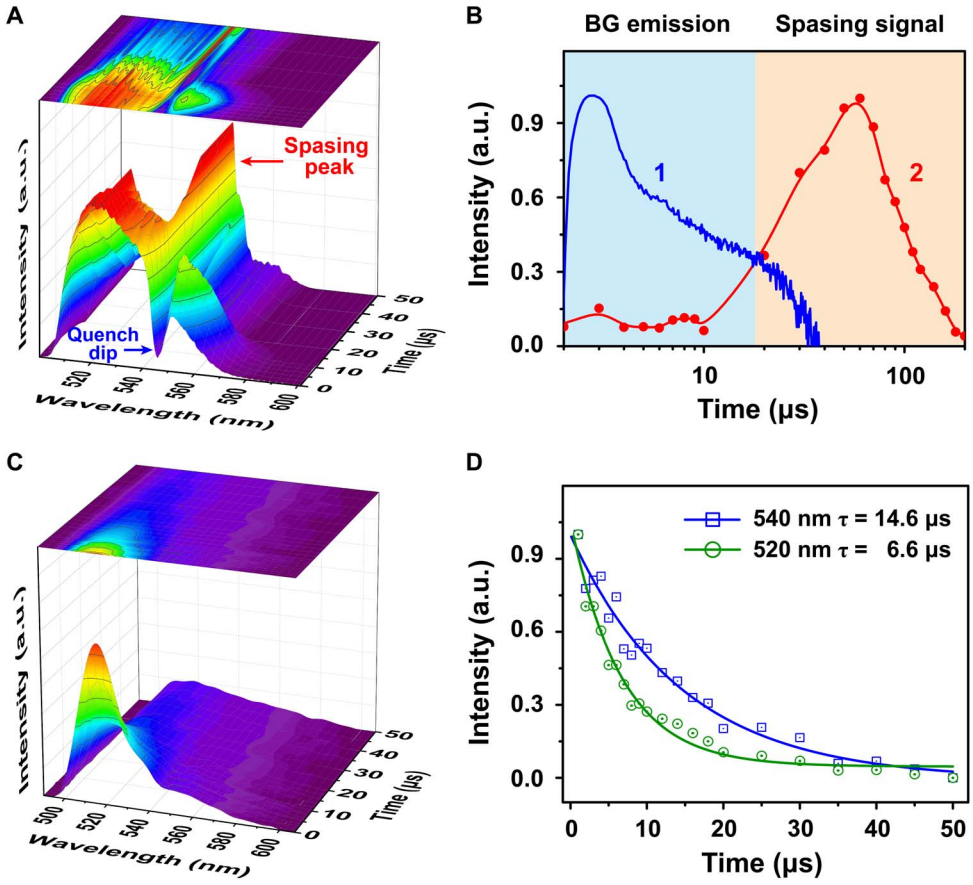

Fig. 3. Delayed spasing dynamics. (**A**) Time-resolved emission spectra of the as-prepared dsDs (temporal resolution, 1 μs). (**B**) Emission dynamics of gain medium itself (line 1) and dsDs (line 2) at 545 nm. BG, background. (**C**) Time-resolved emission spectra of gain material without plasmon cavity. (**D**) Decay curves of emission intensity at 520 and 540 nm, corresponding to delayed fluorescence (τ = 6.6 μs) and phosphorescence (τ = 14.6 μs).

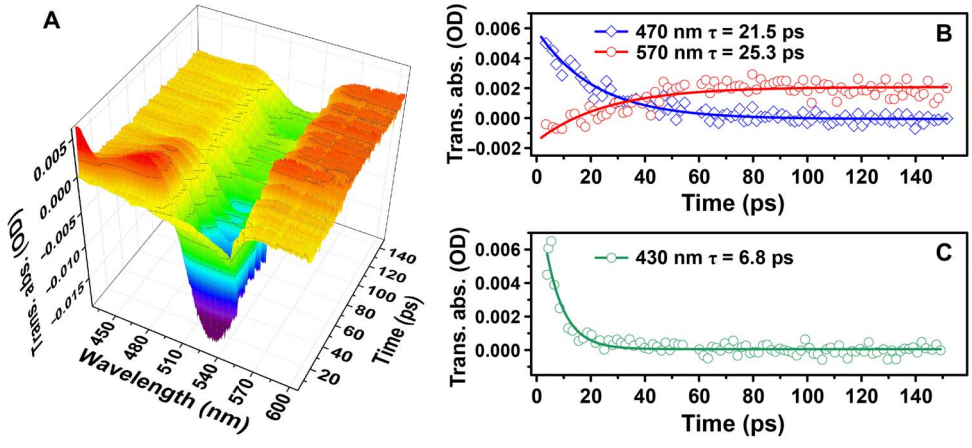

Fig. 4. Electron transition dynamics. (**A**) Picosecond transient absorption spectra of the gain material without plasmon cavity. (**B**) Evolution of transient absorptive signature of $S_1 \rightarrow S_n$ (470 nm, τ = 21.5 ps) and $T_2 \rightarrow T_n$ (570 nm, τ = 25.3 ps) along with time, corresponding to a fast intersystem crossing. (**C**) Decay of transient absorption at 430 nm represents nonradiative relaxation of SiO_2 (τ = 6.8 ps). The dip of about 490 to 530 nm could be attributed to the overlap of ground-state absorption and fluorescence emission. OD, optical density.

The above equations mean that an external excitation pumps electrons from the S_0 state (N_0) to the S_1 state (N_2) at a linear optical pump rate (W_P) that is proportional to the pump light intensity. $\overline{E}\frac{1}{h\omega_{ab}}\frac{\partial P_{ab}}{\partial t}$ represents the nonlinear excitation enhanced by the local field ($\overline{E}$), h is the Planck constant, ω_{ab} is the absorption frequency, and P_{ab} is the net polarization resulting from the local field enhanced absorption. After a short lifetime (τ_{21}), electrons transfer nonradiatively to the T_2 state via intersystem crossing. As mentioned above, dye-doped SiO_2 was used as the gain medium in the current spaser system. The small energy gap (ΔE = 90 meV; fig. S3) between singlet and triplet excited states led to

fast intersystem crossing from the S_1 state to the T_2 state (τ_{21} = 25.3 ps; Fig. 4) and resulted in the accumulation of excited electrons in the T_2 state. The electrons in the T_2 state can transfer to the S_0 state through a radiative path ($1/\tau_{10}$) or to the plasmon cavity through dipole-dipole interaction. $\overline{E}\frac{1}{\hbar\omega_{tr}}\frac{\partial P_{tr}}{\partial t}$ represents the energy transfer enhanced by the local field ($\overline{E}$), ω_{tr} is the transfer frequency, and P_{tr} is the net polaritons resulting from the stimulated energy transfer. At low pump power, the excitation was mainly through $W_P N_0$; when the pump power increased, $\overline{E}\frac{1}{\hbar\omega_{tr}}\frac{\partial P_{tr}}{\partial t}$ quickly dominated the excitation because a large local field density ($\overline{E}$) can remarkably enhance the light absorption on dye molecules and promote the excitation. Because the absorption process is on the femtosecond scale and the intersystem crossing from S_1 to T_2 ($1/\tau_{21}$) is also fast (τ_{21} = 25.3 ps) (*36*), under high pump power, large amount of electrons accumulated in the T_2 state (N_1) and led to large population inversion. In our current spaser system, we doped ~4×10^3 dye molecules into the silica shell per particle, corresponding to a dope intensity of ~0.1/nm^3, and the average distance between dye molecules was estimated to be <3 nm. Under this condition, dipole-dipole interaction between excited molecular dipoles inhibited the spontaneous emission (N_2/τ_{20}, N_1/τ_{10}) and generated a collective polariton coupled to the plasmon oscillation. The coupling between molecular dipole and plasmon polariton resulted in a high-efficiency (~90%) stimulated energy transfer at 545 nm with a linewidth of ~10 nm. This value is much narrower than the linewidth (>50 nm) of absorption spectra from the Au nanoparticles, which suggested a coherent interaction between the gain medium and the plasmon cavity. Notably, in the two-level gain system, the dipole-dipole interaction $\overline{E}\frac{1}{\hbar\omega_{tr}}\frac{\partial P_{tr}}{\partial t}$ caused a reversible energy transfer between molecular dipole and plasmon polariton. Energy transfer from the plasmon polariton to the molecular dipole, referred to as plasmon resonance energy transfer (PRET), might fully quenched the plasmon oscillation in some cases (*38*, *39*). In our three-level gain system, the PRET-mediated energy loss from plasmon polarization to T_2 electrons was eliminated due to the spin forbidden transition from the S_0 state to the T_2 state, and the energy of plasmon oscillation is not enough to excite S_0 electrons to the S_1 state; thus, a quasi-unidirectional energy transfer from the gain medium to the plasmon cavity was generated. Finally, the long excited state lifetime and unidirectional energy transfer resulted in ultralow pump threshold and ultralong lasing lifetime.

CONCLUSION

In summary, we reported a new type of a luminescent nanoprobe based on a three-level spaser. This probe, termed dsDs, about 50 to 60 nm in size, exhibited an emission spectrum of ~3 nm, an ultralow threshold of ~1 mJ cm^{-2}, and a delayed lasing lifetime of ~10^2 μs. Our results suggested that by engineering the energy level of gain materials and regulating the energy transfer between the gain medium and the cavity, the optical property of spasers could be tuned. By designing the energy level of the gain medium and the resonance energy of the plasmon cavity, the lasing wavelength was possibly tunable (*30*, *46*). In addition, a four-level gain system was expected to further reduce the threshold to realize CW-pumped (*11*) and electrically pumped spasing action (*47*, *48*) or to achieve lasing without inversion (*49*). Although our current dsDs are still in their infancy, with the above possibilities, these dsDs open up the way to new-generation luminescent probes for future super-multiplex biological analysis without disturbance of short lifetime background emission.

MATERIALS AND METHODS

Preparation of the spaser nanoprobes

The Au nanoparticles (20 nm) were synthesized using a modified Frens method (*50*). Thin (1 to 2 nm) and dense silica shells were first coated on the Au nanoparticles to avoid coagulation (*51*, *52*). Then, the freshly prepared thin silica-coated Au nanoparticles were transferred to a 20-ml glass bottle containing 2 ml of ultrapure water and 8 ml of ethanol. Under continuous stirring, 10 μl of 3-mercaptopropyltrimethoxysilane (Sigma-Aldrich)–bonded 2′,7′-difluorofluorescein maleimide (4.56 mM; Invitrogen), 1 μl of tetraethoxysilane, and 2 μl of ammonium hydroxide were added to the above solution (*26*). One hour later, the spaser nanoprobes were collected by centrifugal cleaning and redispersed in water. Besides, the control samples of dye-doped SiO_2 and Au@SiO_2 were synthesized without adding Au nanoparticles or dye molecules in the identical condition.

Characteristics

TEM images of the synthesized spaser nanoprobes were characterized on a JEM-1011 transmission electron microscope (JEOL Ltd.). The ultraviolet-visible spectrum of the Au nanoparticles was characterized on a UV-3600 Plus spectrophotometer (Shimadzu Co.). Excitation-emission and luminescence lifetime spectra of the dye molecule were carried on an FLS980 fluorescence spectrometer (Edinburgh Instruments Ltd.).

Broadband time-resolved emission spectroscopy

The optical characteristics of the synthesized spaser nanoprobes were analyzed using a custom-made time-resolved emission spectroscopy system (fig. S1), which is composed of a pulse laser (20 Hz; Quanta-Ray INDI, Spectra-Physics) as the pumping source, a delay generator (DG645, Stanford Research Systems) providing delay and time gate for temporal analysis, and a compact fiber spectrometer (CCS200, Thorlabs Inc.) for collecting the emission spectra.

Transient absorption spectroscopy

Pump-probe experiments were performed with a femtosecond transient absorption spectrometer (ExciPro, CDP Systems Corp.). The pump beam was provided using a femtosecond Ti:sapphire amplifier (1 kHz; Solstice Ace, Spectra-Physics), the pulse width was about 120 fs, and the wavelength was further tuned by an optical parametric amplifier (TOPAS Prime, Spectra-Physics). The probe beam was generated through a supercontinuum crystal to provide a femtosecond pulsed white light with a spectral range of 400 to 800 nm. Resolution of the temporal domain was achieved using an optical delay line with a resolution of about 100 fs. To study the intersystem crossing, the pump wavelength was selected at 400 nm to avoid the absorption band of ground and excited states.

SUPPLEMENTARY MATERIALS

Supplementary material for this article is available at http://advances.sciencemag.org/cgi/content/full/4/8/eaat0292/DC1

Supplementary Text

Instruction of broadband time-resolved emission spectroscopy

Fig. S1. Schematic diagram of broadband time-resolved emission spectroscopy system.

Fig. S2. Molecular modeling of the dye.

Fig. S3. Photoluminescent spectrum measurement.

Fig. S4. Morphology characterization of the control samples.

Fig. S5. Pump-dependent steady-state emission and time-resolved emission spectra of dye solution.

Fig. S6. Electron transition dynamic spectrum of dye solution.

REFERENCES AND NOTES

1. M. Vendrell, D. Zhai, J. C. Er, Y.-T. Chang, Combinatorial strategies in fluorescent probe development. *Chem. Rev.* **112**, 4391–4420 (2012).
2. U. Resch-Genger, M. Grabolle, S. Cavaliere-Jaricot, R. Nitschke, T. Nann, Quantum dots versus organic dyes as fluorescent labels. *Nat. Methods* **5**, 763–775 (2008).
3. K. E. Knowles, K. H. Hartstein, T. B. Kilburn, A. Marchioro, H. D. Nelson, P. J. Whitham, D. R. Gamelin, Luminescent colloidal semiconductor nanocrystals containing copper: Synthesis, photophysics, and applications. *Chem. Rev.* **116**, 10820–10851 (2016).
4. X. Wu, G. Chen, J. Shen, Z. Li, Y. Zhang, G. Han, Upconversion nanoparticles: A versatile solution to multiscale biological imaging. *Bioconjug. Chem.* **26**, 166–175 (2015).
5. B. Zhou, B. Shi, D. Jin, X. Liu, Controlling upconversion nanocrystals for emerging applications. *Nat. Nanotechnol.* **10**, 924–936 (2015).
6. C. H. Contag, M. H. Bachmann, Advances in in vivo bioluminescence imaging of gene expression. *Annu. Rev. Biomed. Eng.* **4**, 235–260 (2002).
7. J. Yao, M. Yang, Y. Duan, Chemistry, biology, and medicine of fluorescent nanomaterials and related systems: New insights into biosensing, bioimaging, genomics, diagnostics, and therapy. *Chem. Rev.* **114**, 6130–6178 (2014).
8. Y. Lu, J. Zhao, R. Zhang, Y. Liu, D. Liu, E. M. Goldys, X. Yang, P. Xi, A. Sunna, J. Lu, Y. Shi, R. C. Leif, Y. Huo, J. Shen, J. A. Piper, J. Paul Robinson, D. Jin, Tunable lifetime multiplexing using luminescent nanocrystals. *Nat. Photonics* **8**, 32–36 (2013).
9. J. Zhang, F. Song, Z. He, Y. Liu, Z. Chen, S. Lin, L. Huang, W. Huang, Wide-range tunable fluorescence lifetime and ultrabright luminescence of Eu-grafted plasmonic core–shell nanoparticles for multiplexing. *Small* **12**, 397–404 (2016).
10. M. Monici, Cell and tissue autofluorescence research and diagnostic applications. *Biotechnol. Annu. Rev.* **11**, 227–256 (2005).
11. W. T. Silfvast, *Laser Fundamentals* (Cambridge Univ. Press, 2004).
12. S. W. Eaton, A. Fu, A. B. Wong, C.-Z. Ning, P. Yang, Semiconductor nanowire lasers. *Nat. Rev. Mater.* **1**, 16028 (2016).
13. M. H. Huang, S. Mao, H. Feick, H. Yan, Y. Wu, H. Kind, E. Weber, R. Russo, P. Yang, Room-temperature ultraviolet nanowire nanolasers. *Science* **292**, 1897–1899 (2001).
14. Y.-C. Chen, X. Tan, Q. Sun, Q. Chen, W. Wang, X. Fan, Laser-emission imaging of nuclear biomarkers for high-contrast cancer screening and immunodiagnosis. *Nat. Biomed. Eng.* **1**, 724–735 (2017).
15. H. Cao, Y. G. Zhao, S. T. Ho, E. W. Seelig, Q. H. Wang, R. P. H. Chang, Random laser action in semiconductor powder. *Phys. Rev. Lett.* **82**, 2278–2281 (1999).
16. B. H. Hokr, J. N. Bixler, M. T. Cone, J. D. Mason, H. T. Beier, G. D. Noojin, G. I. Petrov, L. A. Golovan, R. J. Thomas, B. A. Rockwell, V. V. Yakovlev, Bright emission from a random Raman laser. *Nat. Commun.* **5**, 4356 (2014).
17. Q. Zhang, R. Su, W. Du, X. Liu, L. Zhao, S. Tung Ha, Q. Xiong, Advances in small perovskite-based lasers. *Small Methods* **1**, 1700163 (2017).
18. M. Humar, S. H. Yun, Intracellular microlasers. *Nat. Photonics* **9**, 572–576 (2015).
19. M. A. Noginov, G. Zhu, M. Mayy, B. A. Ritzo, N. Noginova, V. A. Podolskiy, stimulated emission of surface plasmon polaritons. *Phys. Rev. Lett.* **101**, 226806 (2008).
20. D. J. Bergman, M. I. Stockman, Surface plasmon amplification by stimulated emission of radiation: Quantum generation of coherent surface plasmons in nanosystems. *Phys. Rev. Lett.* **90**, 027402 (2003).
21. R.-M. Ma, R. F. Oulton, V. J. Sorger, X. Zhang, Plasmon lasers: Coherent light source at molecular scales. *Laser Photonics Rev.* **7**, 1–21 (2013).
22. R. F. Oulton, V. J. Sorger, T. Zentgraf, R.-M. Ma, C. Gladden, L. Dai, G. Bartal, X. Zhang, Plasmon lasers at deep subwavelength scale. *Nature* **461**, 629–632 (2009).
23. R.-M. Ma, R. F. Oulton, V. J. Sorger, G. Bartal, X. Zhang, Room-temperature sub-diffraction-limited plasmon laser by total internal reflection. *Nat. Mater.* **10**, 110–113 (2010).
24. Y.-J. Lu, J. Kim, H.-Y. Chen, C. Wu, N. Dabidian, C. E. Sanders, C.-Y. Wang, M.-Y. Lu, B.-H. Li, X. Qiu, W.-H. Chang, L.-J. Chen, G. Shvets, C.-K. Shih, S. Gwo, Plasmonic nanolaser using epitaxially grown silver film. *Science* **337**, 450–453 (2012).
25. Y.-H. Chou, B.-T. Chou, C.-K. Chiang, Y.-Y. Lai, C.-T. Yang, H. Li, T.-R. Lin, C.-C. Lin, H.-C. Kuo, S.-C. Wang, T.-C. Lu, Ultrastrong mode confinement in ZnO surface plasmon nanolasers. *ACS Nano* **9**, 3978–3983 (2015).
26. M. A. Noginov, G. Zhu, A. M. Belgrave, R. Bakker, V. M. Shalaev, E. E. Narimanov, S. Stout, E. Herz, T. Suteewong, U. Wiesner, Demonstration of a spaser-based nanolaser. *Nature* **460**, 1110–1112 (2009).
27. K. G. Stamplecoskie, M. Grenier, J. C. Scaiano, Self-assembled dipole nanolasers. *J. Am. Chem. Soc.* **136**, 2956–2959 (2014).
28. E. I. Galanzha, R. Weingold, D. A. Nedosekin, M. Sarimollaoglu, J. Nolan, W. Harrington, A. S. Kuchyanov, R. G. Parkhomenko, F. Watanabe, Z. Nima, A. S. Biris, A. I. Plekhanov, M. I. Stockman, V. P. Zharov, Spaser as a biological probe. *Nat. Commun.* **8**, 15528 (2017).
29. E. I. Galanzha, R. Weingold, D. A. Nedosekin, M. Sarimollaoglu, A. S. Kuchyanov, R. G. Parkhomenko, A. I. Plekhanov, M. I. Stockman, V. P. Zharov, Spaser as novel versatile biomedical tool. http://arxiv.org/abs/1501.00342 (2015).
30. X. Meng, A. V. Kildishev, K. Fujita, K. Tanaka, V. M. Shalaev, Wavelength-tunable spasing in the visible. *Nano Lett.* **13**, 4106–4112 (2013).
31. T. V. Shahbazyan, Mode volume, energy transfer, and spaser threshold in plasmonic systems with gain. *ACS Photonics* **4**, 1003–1008 (2017).
32. M. I. Stockman, The spaser as a nanoscale quantum generator and ultrafast amplifier. *J. Opt.* **12**, 024004 (2010).
33. B. Min, E. Ostby, V. Sorger, E. Ulin-Avila, L. Yang, X. Zhang, K. Vahala, High-Q surface-plasmon-polariton whispering-gallery microcavity. *Nature* **457**, 455–458 (2009).
34. Y. Li, J. Zhang, D. Huang, H. Sun, F. Fan, J. Feng, Z. Wang, C. Z. Ning, Room-temperature continuous-wave lasing from monolayer molybdenum ditelluride integrated with a silicon nanobeam cavity. *Nat. Nanotechnol.* **12**, 987–992 (2017).
35. K. E. Dorfman, P. K. Jha, D. V. Voronine, P. Genevet, F. Capasso, M. O. Scully, Quantum-coherence-enhanced surface plasmon amplification by stimulated emission of radiation. *Phys. Rev. Lett.* **111**, 043601 (2013).
36. B. Valeur, M. N. Berberan-Santos, *Molecular Fluorescence: Principles and Applications* (John Wiley & Sons, 2013).
37. P. Berini, I. De Leon, Surface plasmon–polariton amplifiers and lasers. *Nat. Photonics* **6**, 16–24 (2012).
38. Y. Choi, T. Kang, L. P. Lee, Plasmon resonance energy transfer (PRET)-based molecular imaging of cytochrome c in living cells. *Nano Lett.* **9**, 85–90 (2009).
39. G. L. Liu, Y.-T. Long, Y. Choi, T. Kang, L. P. Lee, Quantized plasmon quenching dips nanospectroscopy via plasmon resonance energy transfer. *Nat. Methods* **4**, 1015–1017 (2007).
40. T. V. Shahbazyan, Local density of states for nanoplasmonics. *Phys. Rev. Lett.* **117**, 207401 (2016).
41. W. Zhou, M. Dridi, J. Yong Suh, C. Hoon Kim, D. T. Co, M. R. Wasielewski, G. C. Schatz, T. W. Odom, Lasing action in strongly coupled plasmonic nanocavity arrays. *Nat. Nanotechnol.* **8**, 506–511 (2013).
42. E. M. Purcell, H. C. Torrey, R. V. Pound, Resonance absorption by nuclear magnetic moments in a solid. *Phys. Rev.* **69**, 37–38 (1946).
43. S. Wuestner, A. Pusch, K. L. Tsakmakidis, J. M. Hamm, O. Hess, Overcoming losses with gain in a negative refractive index metamaterial. *Phys. Rev. Lett.* **105**, 127401 (2010).
44. J. M. Hamm, S. Wuestner, K. L. Tsakmakidis, O. Hess, Theory of light amplification in active fishnet metamaterials. *Phys. Rev. Lett.* **107**, 167405 (2011).
45. X.-L. Zhong, Z.-Y. Li, All-analytical semiclassical theory of spaser performance in a plasmonic nanocavity. *Phys. Rev. B* **88**, 085101 (2013).
46. Z. Wang, X. Meng, A. V. Kildishev, A. Boltasseva, V. M. Shalaev, Nanolasers enabled by metallic nanoparticles: From spasers to random lasers. *Laser Photonics Rev.* **11**, 1700212 (2017).
47. D. Li, M. I. Stockman, Electric spaser in the extreme quantum limit. *Phys. Rev. Lett.* **110**, 106803 (2013).
48. B. Liu, W. Zhu, S. D. Gunapala, M. I. Stockman, M. Premaratne, Open resonator electric spaser. *ACS Nano* **11**, 12573–12582 (2017).
49. S. E. Harris, Lasers without inversion: Interference of lifetime-broadened resonances. *Phys. Rev. Lett.* **62**, 1033–1036 (1989).
50. G. Frens, Controlled nucleation for the regulation of the particle size in monodisperse gold suspensions. *Nat. Phys. Sci.* **241**, 20–22 (1973).
51. L. M. Liz-Marzán, M. Giersig, P. Mulvaney, Synthesis of nanosized gold–silica core–shell particles. *Langmuir* **12**, 4329–4335 (1996).
52. J. F. Li, Y. Fan Huang, Y. Ding, Z. Lin Yang, S. Bo Li, X. Shun Zhou, F. Ru Fan, W. Zhang, Z. You Zhou, D. Yin Wu, B. Ren, Z. Lin Wang, Z. Qun Tian, Shell-isolated nanoparticle-enhanced Raman spectroscopy. *Nature* **464**, 392–395 (2010).

Acknowledgments

Funding: This work was mainly supported by the National Natural Science Foundation of China (21327902, 21675081, and 21535003), State Key Laboratory of Analytical Chemistry for Life Science (5431ZZXM1715), National Key R&D Program of China (2016YFA0201200), and Priority Academic Program Development of Jiangsu Higher Education Institutions. **Author contributions:** H.-Y.C., J.-J.X., and B.K. conceived the research. B.K. designed and built the spectroscopy system. P.S. and J.-H.W. performed the experiments. M.Z. contributed to instrumentation operation. H.-J.L. and F.Y. contributed to sample preparation. P.S., B.K., and J.-J.X. wrote the manuscript. All authors discussed the results and commented on the manuscript. **Competing interests:** The authors declare that they have no competing interests. **Data and materials availability:** All data needed to evaluate the conclusions in the paper are present in the paper and/or the Supplementary Materials. Additional data related to this paper may be requested from the authors.

Submitted 17 January 2018
Accepted 11 July 2018
Published 17 August 2018
10.1126/sciadv.aat0292

Citation: P. Song, J.-H. Wang, M. Zhang, F. Yang, H.-J. Lu, B. Kang, J.-J. Xu, H.-Y. Chen, Three-level spaser for next-generation luminescent nanoprobe. *Sci. Adv.* **4**, eaat0292 (2018).

Science Advances

Three-level spaser for next-generation luminescent nanoprobe

Pei Song, Jian-Hua Wang, Miao Zhang, Fan Yang, Hai-Jie Lu, Bin Kang, Jing-Juan Xu and Hong-Yuan Chen

Sci Adv **4** (8), eaat0292.
DOI: 10.1126/sciadv.aat0292